J Therm Anal Calorim (2012) 107:325–334
DOI 10.1007/s10973-011-1781-5

Preparation, X-ray crystallography and thermolysis of transition metal nitrates of 2,2′-bipyridine (Part 63)

Dinesh Kumar · Inder Pal Singh Kapoor · Gurdip Singh · Nidhi Goel · Udai Pratap Singh

Received: 23 September 2010 / Accepted: 29 June 2011 / Published online: 11 August 2011

Abstract Recent work has described the preparation and characterization of the two complexes $[Fe_2(C_{10}H_8N_2)_4O(OH_2)_2](NO_3)_4$ and $[Co(C_{10}H_8N_2)_3]_2[Co(OH_2)_6]\cdot 7(OH_2)(NO_3)_8$ in which both the nitrogen atoms of 2,2′-bipyridine are directly bonded with the metals. Their structures were determined by single-crystal X-ray diffraction at 296 K. Thermolysis of these complexes has been detailed by the use of TG–DTA and ignition delay measurements. Kinetics of thermal decomposition has also been established. Model free isoconversional and model fitting kinetic approaches have been applied to isothermal TG data for the decomposition of these complexes.

Keywords 2,2′-bipyridine · Isoconversional · Ignition delay · Isothermal TG · Thermolysis · Iron and cobalt complexes

Introduction

Interest is growing in the complexes of transition metals having NO_3^- or ClO_4^- anions as oxidizer and ethylenediamine [1, 2], propylenediamine [3, 4], 1,4-diaminobutane [5, 6], hexamethylenetetramine [7, 8], and 1,6-diaminohexane [9] as reducing groups. These complexes are well-known for their exothermic autocatalytic thermal decomposition. Thus, they are of interest as rocket propellants and explosives [10]. When subjected to high temperature, these complexes undergo exothermic self-propagative decomposition reactions leading to ignition and produce highly thermally stable residue most closely resemble corresponding metal oxide as is consistent with their thermal decomposition behavior. These oxides can be utilized as burning rate catalysts. Frazer and Hicks [11, 12] proposed the thermal ignition model where heat of reaction is taken to be a function of temperature. The heat liberated due to exothermic reaction leads to deflagration. It is well-known that when a solid material deflagrates, a steep temperature gradient is produced at the surface [13]. The surface region can be thought of as a thin film of material where heat and mass transfer are driven by physico-chemical changes. The reaction zone in the condensed phase (which may be a solid phase) is thin, transient, and non-isothermal. Reactions in the condensed phase liberate gaseous products for ignition. In our earlier publications [14–16], it has been possible to gain insight into the mechanism of preignition reactions by using tube furnace (TF) and thermogravimetric (TG) technique where deflagration conditions are simulated.

Very recently, we have also demonstrated the preparation, characterization, and kinetics of thermolysis of transition metal perchlorates with 1,6-diaminohexane [17] and 2,2′-bipyridyl ligands [18]. In the light of the above findings, it was decided to synthesize, characterize, and undertake a systematic investigation on thermal and ignition characteristics of iron and cobalt nitrate complexes of 2,2′-bipyridine.

D. Kumar · I. P. S. Kapoor · G. Singh (✉)
Department of Chemistry, DDU Gorakhpur University, Gorakhpur 273009, India
e-mail: gsingh4us@yahoo.com

N. Goel · U. P. Singh
Department of Chemistry, IIT, Roorkee 247667, India

Experimental

Materials

Cobalt carbonate, ethanol, and nitric acid were obtained from s.d. fine. Ferric nitrate and 2,2′-bipyridine were purchased from Qualigens. Petroleum ether was obtained from Merck. All the materials were used without further purification.

Preparation

The complex $[Fe_2(C_{10}H_8N_2)_4O(OH_2)_2](NO_3)_4$ was prepared by the reaction of ethanolic solution of ferric nitrate and 2,2′-bipyridine at room temperature. The mixture was stirred and filtered. The complex was crystallized from the filtrate by slow evaporation. Recrystallisation of the crude product from aqueous solution gave the complex as a brown crystalline solid [yield 67%, m.p. 198 °C(d)]. Caution! Here the synthesized complexes are sensitive explosives, ignite on rapid heating, and should be handled with care.

Compound $[Co(C_{10}H_8N_2)_3]_2[Co(OH_2)_6]\cdot 7(OH_2)(NO_3)_8$ was prepared by adding 2,2′-bipyridine to the ethanolic solution of cobalt nitrate in the same conditions as for the iron complex. Cobalt nitrate was prepared by the same method as reported earlier [7]. The resulting cobalt nitrate was washed with petroleum ether, recrystallized from distilled water and air-dried. The complex was purified by recrystallization from aq. solution as brown crystals [yield 70%, m.p. > 200 °C (d)].

Characterization

The single crystal X-ray structure of $[Fe_2(C_{10}H_8N_2)_4O(OH_2)_2](NO_3)_4$ and $[Co(C_{10}H_8N_2)_3]_2[Co(OH_2)_6]\cdot 7(OH_2)(NO_3)_8$ were determined on crystals obtained from the high concentration of aqueous solutions of the respective complexes. Single crystal X-ray diffraction data were collected at 296 K on a Bruker Kappa-CCD diffaractometer using graphite monochromated Mo-Kα radiation (k = 0.71073 Å). The structures were solved by the direct methods. Structure solutions, refinement, and data output were carried out with SHELX TL program [19, 20]. Non-hydrogen atoms were refined anisotropically; all non hydrogen atoms were refined anisotropically without constraint. Images were created with the DIAMOND and MERCURY program [21, 22]. The crystal structure with hydrogen bonding interactions of the complexes are shown in Figs. 1, 2, 3 and 4. Crystal and refinement parameters, bond lengths, bond angle, and hydrogen bonding interactions, respectively, are summarized in Tables 1, 2 and 3. The CCDC No. for Fe and Co complexes are, respectively, 757103 and 757102. IR spectroscopy studies were conducted with PERKIN ELMER; FT–IR Spectrometer with resolution of 1.0 cm^{-1} (Table 4). X-ray diffraction (XRD) of oxides were performed on XPERTPro PANalytical instrument between the 2θ ranges of 10–110° (Fig. 5).

Thermal analysis

Thermogravimetry and differential thermal analysis (TG–DTA) were performed on NETZCHSTA 409C/CD instrument analyzer. 0.10 mg of sample was used and heating rate was 10 °C per minute (Table 5). In addition, nitrogen flow rate of 96 mL/min was present and the traces are shown in Fig. 6. Isothermal TG was performed at appropriate temperatures in static air (mass 20 mg) with an indigenous fabricated TG apparatus [23] using gold crucible as a sample holder and traces are shown in Fig. 7.

The ignition delay (D_i) or time ignition delay (t_{id}) measurements were made on 20 mg samples (100–200 mesh) by using a tube furnace technique (TF) [15] in the

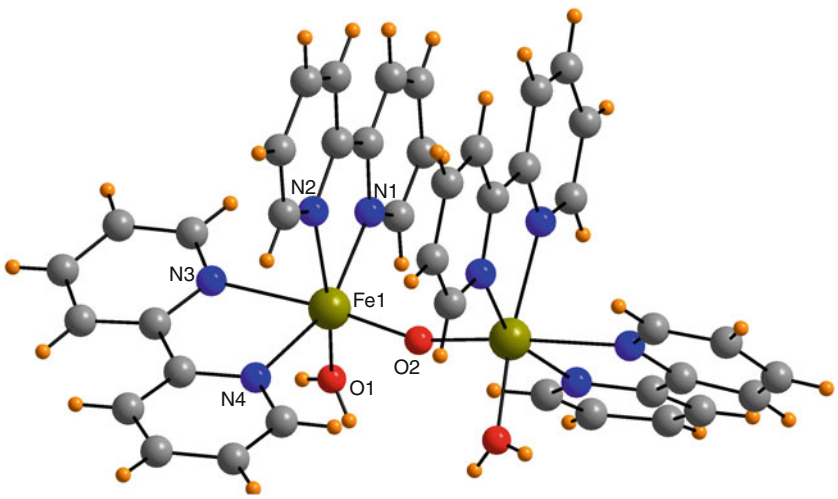

Fig. 1 Crystal structure (ball and stick model) of iron complex $[Fe_2(C_{10}H_8N_2)_4O(OH_2)_2](NO_3)_4$ complex. Four nitrate ions, present in lattice have been omitted for clarity

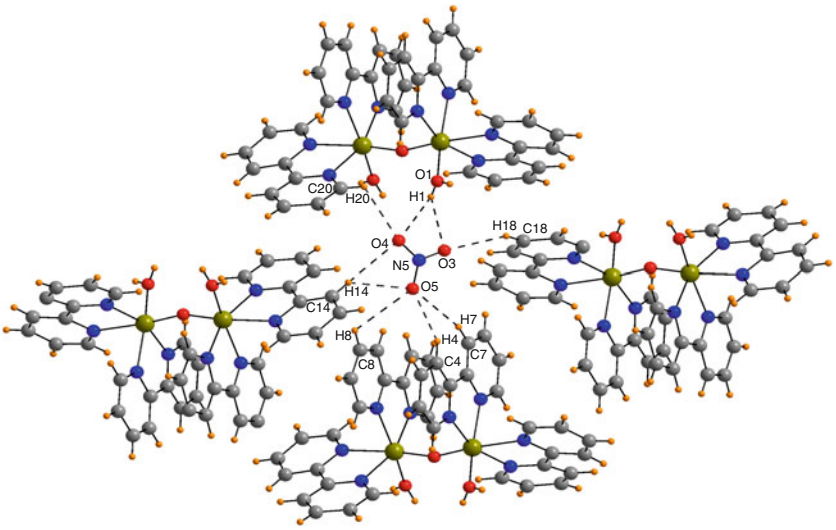

Fig. 2 Figure showing C–H···O and O–H···O intermolecular interactions in iron complex

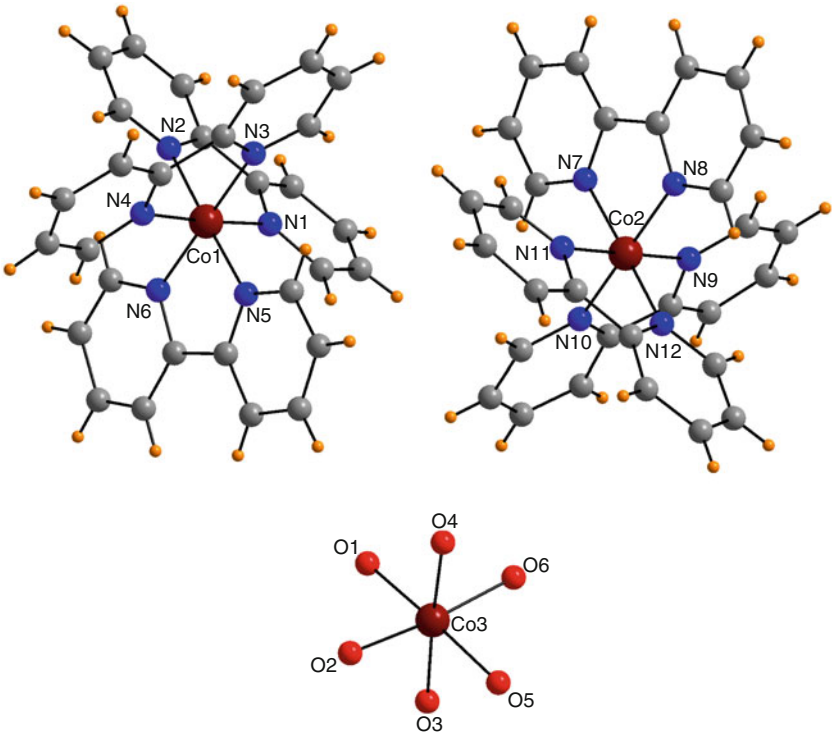

Fig. 3 Crystal structure (ball and stick model) of cobalt complex $[Co(C_{10}H_8N_2)_3]_2[Co(OH_2)_6]\cdot 7(OH_2)(NO_3)_8$ complex. Eight nitrate ions and seven water molecules present in lattice have been omitted for clarity

temperature range of 290–390 °C. The accuracy of the temperature of the tube furnace was ±1 °C. The sample was taken in an ignition tube (0.5 cm diameter × 4.5 cm length) and the time interval between the insertion of the ignition tube into the TF and the moment of appearance of a flame noted with the help of a stop watch with the accuracy of ±0.1 s, gave the value of ignition delay (t_{id}). The ignition tube, clamped in a bent wire, was inserted manually into the furnace up to a fix depth (14 cm) just above the probe of the temperature indicator cum controller (Century, Chandigarh). The time for insertion of the ignition tube was also kept constant. Each run was repeated three times, and mean t_{id} values are reported in Table 6. The t_{id} data were found to be fit in equation, [24–26]

$$t_{id} = Ae^{E_a/RT} \quad (1)$$

where t_{id} is the time of ignition (ignition delay), A is a constant, E_a is the energy of activation for ignition, and T is the absolute temperature. A plot depicting the relation between $\ln t_{id}$ and $1/T$ for the complexes is shown in Fig. 8. This equation has been found to be obeyed by a large number of explosives [7, 8, 14, 18, 27, 28].

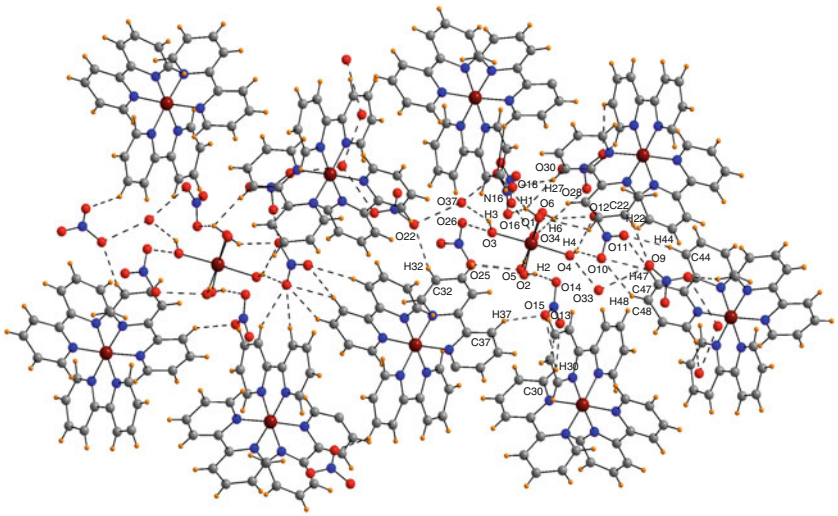

Fig. 4 Figure showing C–H···O and O–H···O intermolecular interactions in cobalt complex

Table 1 Crystal data and structure refinement for Fe and Co complexes

Complex designation	Fe complex	Co complex
Empirical formula	$C_{40}H_{36}Fe_2N_{12}O_{15}$	$C_{60}H_{54}\ Co_3N_{20}\ O_{37}^{a}$
Color	Brown	Brown
Formula weight	1036.51	1824.02
Temp/K	296(2)	296(2)
λ/A^0	0.71073	0.71073
Crystal system	Monoclinic	Monoclinic
Space group	C 2/c	P n
Unit cell dimensions	$a = 22.576(2)$ Å, $\alpha = 90^{\circ}$	a = 17.278(3) Å, $\alpha = 90.000°$
	$b = 12.723(2)$ Å, $\beta = 124.471(4)°$	b = 9.8136(16) Å, $\beta = 105.012(10)°$
	$c = 18.116(3)$ Å, $\gamma = 90°$	c = 23.327(5)A, $\gamma = 90.00°$
Volume	4289.9(9) Å^3	3820.3(12) Å^3
Molecules per unit cell, Z	4	2
Calculated density	1.605 Mg/m^3	1.586 Mg/m^3
Absorption coefficient	0.763 mm^{-1}	0.571 mm^{-1}
Crystal size/mm	0.27 × 0.23 × 0.19	0.28 × 0.21 × 0.13
Refinement method	Full-matrix least-squares on F^2	Full-matrix least-squares on F^2
θ range for data collection	1.94–28.42^0	1.32–26.71^0
Radiation	Mo Kα	Mo Kα
Goodness-off-fit on F^2	1.191	1.079
Final R indices [I > 2σ(I)]	0.0436	0.0504
CCDC No.	757103	757102

[a] Hydrogen is not added on water molecules, coordinated to the metal center (Co3) and freely present in lattice but has been shown in the formula to remove the confusion

Results and discussion

The crystal data and details of data collection together with the refinement procedure of both Fe and Co complexes at 296 K are given in Table 1. In addition Table 4 pertains the frequencies and assignments for the mid–IR absorptions [29] of the complexes. The structure analysis of the dinuclear complex of $[Fe_2(C_{10}H_8N_2)_4O(OH_2)_2](NO_3)_4$ showed that this complex crystallizes in the monoclinic space group C2/c ($Z = 4$) and its molecular structure is shown in Fig. 1. In this crystal structure each iron atom is hexa coordinated with the coordination polyhedron close to octahedral. Though, the octahedral geometry is achieved by the coordination of four nitrogen atoms (N1, N2, N3, N4 of bipyridine), oxygen atom (O1) of water molecule and one oxygen atom from bridged oxo (O2). Nevertheless,

Table 2 Bond lengths (Å) and angles (°) for Fe and Co complexes

Fe complex				Co complex			
Bond	Length	Bond	Angle	Bond	Length	Bond	Angle
Fe1–O1	2.015(4)	O2–Fe1–O1	95.42(12)	Co1–N1	1.926(10)	N1–Co1–N2	82.45(31)
Fe1–O2	1.786(2)	O2–Fe1–N4	97.93(11)	Co1–N2	1.973(10)	N1–Co1–N3	94.31(36)
Fe1–N1	2.138(5)	O1–Fe1–N4	96.37(11)	Co1–N3	1.944(12)	N1–Co1–N4	176.98(36)
Fe1–N2	2.173(3)	O2–Fe1–N1	99.14(11)	Co1–N4	1.952(10)	N3–Co1–N2	86.65(35)
Fe1–N3	2.230(5)	O1–Fe1–N1	93.12(11)	Co1–N5	1.916(9)	N3–Co1–N4	83.26(37)
Fe1–N4	2.129(5)	N4–Fe1–N1	159.56(11)	Co1–N6	1.914(12)	N4–Co1–N2	95.59(35)
O2–Fe1^{i}	1.786(2)	O2–Fe1–N2	97.12(10)	Co2–N6	1.950(11)	N4–Co1–N5	87.42(11)
		O1–Fe1–N2	164.41(11)	Co2–N7	1.950(1)	N5–Co1–N1	93.52(31)
		N4–Fe1–N2	91.04(10)	Co2–N8	1.943(12)	N5–Co1–N2	175.88(30)
		N1–Fe1–N2	75.79(10)	Co2–N9	1.93(1)	N5–Co1–N3	94.57(34)
		O2–Fe1–N3	172.68(11)	Co2–N1	1.901(11)	N5–Co1–N4	88.47(35)
		O1–Fe1–N3	84.20(14)	Co2–N11	1.95(1)	N6–Co1–N1	88.02(36)
		N4–Fe1–N3	74.88(12)	Co2–N12	1.902(11)	N6–Co1–N2	95.30(35)
		N1–Fe1–N3	88.17(13)	Co3–O1	2.071(10)	N6–Co1–N3	177.14(38)
		N2–Fe1–N3	84.53(12)	Co3–O2	2.092(11)	N6–Co1–N4	94.46(38)
		Fe1–O2–Fe1^{i}	160.78(3)	Co3–O3	2.099(12)	N6–Co1–N5	83.63(34)
				Co3–O4	2.085(12)	N8–Co2–N7	83.80(38)
				Co3–O5	2.120(11)	N8–Co2–N11	86.22(36)
				Co3–O6	2.107(11)	N9–Co2–N7	87.24(38)
						N9–Co2–N8	93.53(38)
						N9–Co2–N11	179.72(37)
						N10–Co2–N7	93.78(34)
						N10–Co2–N8	176.08(36)
						N10–Co2–N9	83.25(37)
						N10–Co2–N11	97.00(35)
						N11–Co2–N7	92.86(35)
						N12–Co2–N7	176.11(38)
						N12–Co2–N8	94.88(38)
						N12–Co2–N9	96.51(37)
						N12–Co2–N10	87.73(34)
						N12–Co2–N11	83.39(34)
						O1–Co3–O2	87.42(35)
						O1–Co3–O3	93.41(37)
						O1–Co3–O4	89.99(38)
						O1–Co3–O5	176.99(36)
						O1–Co3–O6	90.23(35)
						O2–Co3–O3	92.27(34)
						O2–Co3–O5	92.44(34)
						O2–Co3–O6	174.12(33)
						O3–Co3–O5	83.59(35)
						O3–Co3–O6	93.25(35)
						O4–Co3–O2	88.74(34)
						O4–Co3–O3	176.49(37)
						O4–Co3–O5	93.01(35)
						O4–Co3–O6	85.88(35)
						O6–Co3–O5	90.19(36)

Symmetry transformations used to generate equivalent atoms

Table 3 Hydrogen bonding geometry (Å) for Fe and Co complexes

D–H···A	d(D–H)	d(H–A)	d(D–A)	⟨(DHA)⟩
Complex (1)				
O1–H1···O4	0.821(3)	2.216(4)	2.864(6)	136.04(22)
O1–H1···O3	0.821(3)	2.369(7)	3.078(8)	145.02(26)
C4–H4···O5	0.930(4)	2.339(5)	3.264(6)	154.64(26)
C7–H7···O5	0.930(4)	2.803(7)	3.706(8)	164.35(27)
C8–H8···O5	0.930(5)	2.924(8)	3.470(9)	118.89(33)
C14–H14···O4	0.929(5)	2.624(5)	3.537(8)	167.36(28)
C14–H14···O5	0.929(5)	2.598(8)	3.313(10)	134.18(31)
C18–H18···O3	0.930(5)	2.433(7)	3.090(9)	127.64(31)
C20–H20···O4	0.929(6)	2.616(4)	3.157(7)	117.68(29)
Complex (2)				
O1–H1···O16	0.820(11)	2.361(12)	2.834(16)	117.47(72)
O1–H1···O17	0.820(11)	2.864(13)	3.605(16)	151.16(76)
O2–H2···O14	0.829(14)	1.969(14)	2.764(17)	163.28(73)
O3–H3···O37	0.820(9)	2.046(11)	2.764(14)	146.14(69)
O4–H4···O12	0.829(9)	2.597(10)	3.350(13)	153.05(65)
O6–H6···O12	0.820(9)	2.193(12)	2.910(16)	146.08(69)
C22–H22···O9	0.929(13)	2.461(15)	3.344(20)	158.70(88)
C23–H23···O1	0.930(12)	2.960(14)	3.579(21)	125.38(0)
C30–H30···O13	0.930(12)	2.545(19)	3.308(23)	139.51(78)
C32–H32···O22	0.930(12)	2.393(17)	3.251(21)	153.35(83)
C37–H37···O15	0.930(14)	2.321(17)	3.147(23)	147.77(92)
C40–H40···O17	0.932(14)	2.706(18)	3.503(24)	144.00(87)
C44–H44···O11	0.931(12)	2.588(14)	3.509(19)	169.93(70)
C47–H47···O10	0.931(12)	2.616(13)	3.223(18)	123.28(79)
C48–H48···O10	0.929(12)	2.659(9)	3.257(14)	122.81(70)

coordinated water and one nitrogen atom of bipyridine are trans with respect to the N2ON plane. The interest in this system focuses on the interaction of one NO_3^- anion with four $[Fe_2(C_{10}H_8N_2)_4O(OH_2)_2]$ units. The Fe–O bond distances fall in the range of 1.786(2)–2.015(2) Å where Fe–O2 bond distance is lesser than Fe–O1 (2.16 Å is reported in the literature) [30] which is due to the bridged oxo. In addition the Fe–N bond distances are in the range of 2.129(5)–2.230(5) Å (Table 2). The crystal packing shows that the hydrogen atoms of the coordinated water molecule (O1) are involved in hydrogen bonding with the oxygen atom of the uncoordinated nitrate ion (O3, O4) via O–H···N [O1–H1···O3, 2.369(7) Å; O1–H1···O4, 2.216(4) Å] as while the oxygen atoms (O3, O4, O5) of un-coordinated nitrate molecule preclude significant C–H···O [C4–H4···O5, 2.339(5) Å; C7–H7···O5, 2.803(7) Å; C8–H8···O5, 2.924(8) Å; C14–H14···O4, 2.624(5) Å; C14–H14···O5, 2.598(8) Å; C18–H18···O3, 2.433(7) Å; C20–H20···O4, 2.616(4) Å] intermolecular interactions with hydrogen atoms of co-coordinated bipyridine moiety, i.e., hydrogen-bonded networks help to stabilize the crystal structure as shown in Fig. 2 and Table 3.

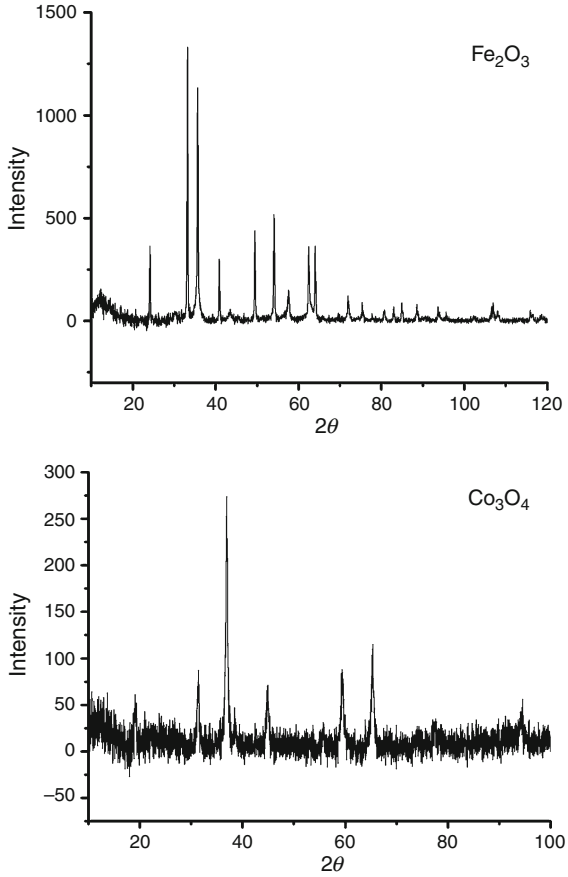

Fig. 5 X-ray diffraction (XRD) pattern of oxides left after decomposition of the complexes

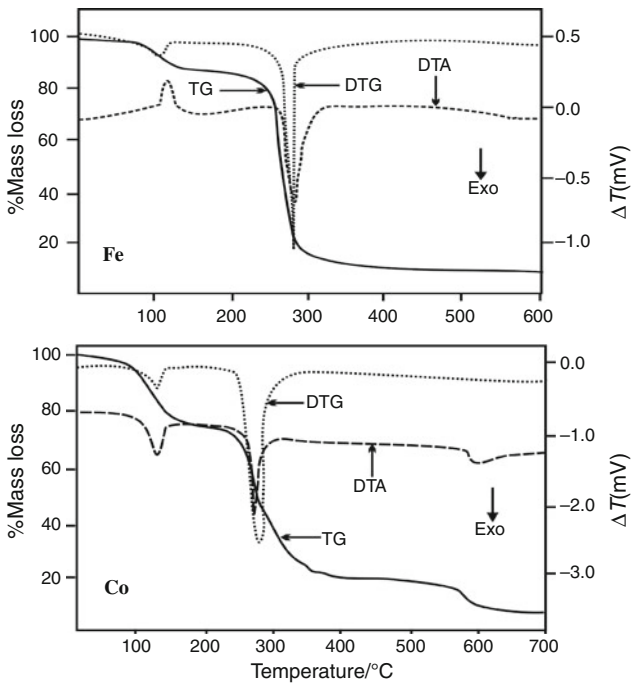

Fig. 6 TG–DTA thermograms in nitrogen atmosphere

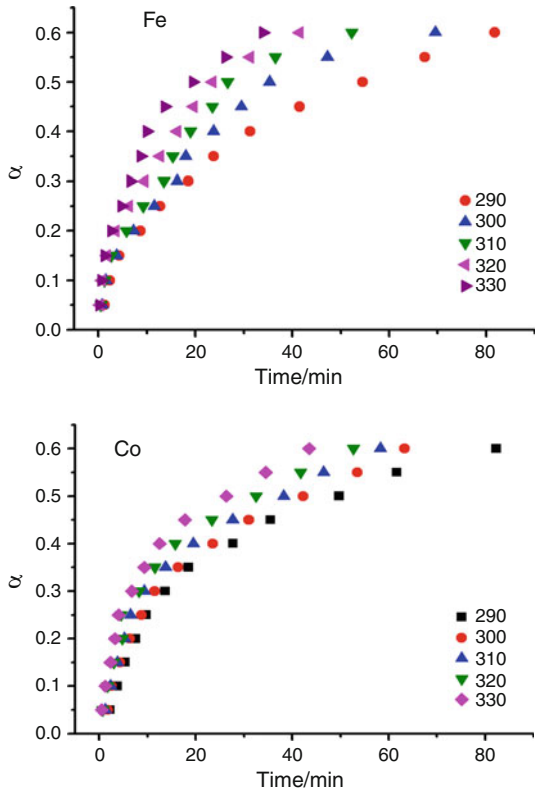

Fig. 7 Isothermal TG of complexes in static air

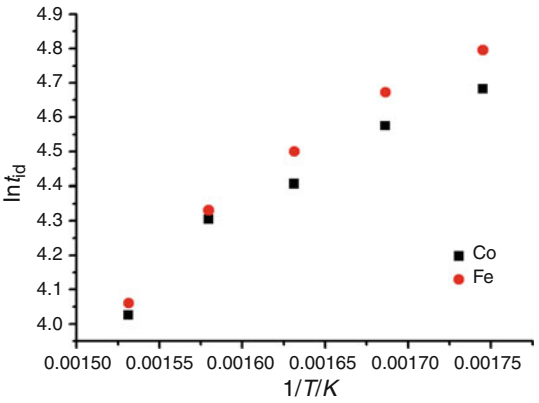

Fig. 8 Plot showing variation of lnt_{id} against $1/T$ for the complexes

The infrared spectrum of Fe-complex was recorded at room temperature and the observed frequencies and the assignments are listed in Table 4. The absorption peak near 3391 cm^{-1} indicates that there are hydrogen bonds in this complex. The bands at 2926 and 899 cm^{-1} are due to, respectively, asymmetric C–H stretching and out-of-plane C–H def. modes. A metal-ligand stretching band occurs in the far infrared range. A strong peak at 633 cm^{-1} could be assigned to the Fe–N stretching mode. The absorption at 1599 cm^{-1} is assigned to νC=C bond while νC=N is assigned to the 1509 cm^{-1}. νC–C and νC–N are easily assigned fundamentals, respectively, at 1288 and 1043 cm^{-1}. The stretching of nitrate anion appears at reasonably well-defined mode at 1385 cm^{-1}.

Table 4 Mid-IR frequencies for Fe and Co complexes

Fe complex		Co complex	
ν cm^{-1}	Assignments	ν cm^{-1}	Assignments
633	M–N	726	M–N
899	C–H def.	889	C–H def.
1043	C–N	1038	C–N
1288	C–C	1174	C–C/sym
1385	NO_3^-	1311	NO_3^-
1472	C–H/sym.	1573	C=N
1509	C=N	1634	C=C
1599	C=C	2571	C–C str/asy.
2926	C–H str/asy.	3406	H-bonding
3391	H-bonding		

The crystal structure of Cobalt complex, $[Co(C_{10}H_8N_2)_3]_2[Co(OH_2)_6]\cdot 7(OH_2)\ (NO_3)_8$, was also determined by the single crystal X-ray diffraction and the atom labeling scheme is shown in Fig. 3. This complex crystallizes in monoclinic, Pn space group. In addition, three bipyridine moieties through six nitrogen (sp^2 hybridized) atoms (N1,N2,N3,N4,N5,N6) are coordinated to Co1 while other six nitrogen atoms (N7,N8,N9,N10,N11,N12) are coordinated with Co2. The third cobalt atom Co3 of the complex contains six coordinated water molecules to achieve octahedral geometry. There are eight nitrates and seven water molecules are freely present in the lattice. An extensive network of C–H···O [C23–H23···O1, 2.960(14) Å; C30–H30···O13, 2.545(19) Å; C32–H32···O22, 2.393(17) Å; C37–H37···O15, 2.321(17) Å; C40–H40···O17, 2.706(18) Å; C44–H44···O11, 2.588(14) Å; C47–H47···O10, 2.616(13) Å; C48–H48···O10, 2.659(9) Å] and O–H···O [O1–H1···O16, 2.361(12) Å; O1–H1···O17, 2.864(13) Å; O2–H2···O14, 1.969(14) Å; O3–H3···O37, 2.046(11) Å; O4–H4···O12, 2.597(10) Å; O6–H6···O12, 2.193(12) Å; C22–H22···O9, 2.461(15) Å] contacts are, of course, essential for lattice packing (Fig. 4, Table 3).

In the region of νO–H stretching, the broad absorption bands at 3406 cm^{-1} suggest hydrogen bonding in the Co complex (Table 4). The band at 889 cm^{-1} is due to the out-of-plane C–H deformation. Absorption at 726 cm^{-1} could be attributed to Co–N stretching. The absorption at 1634 cm^{-1} is assigned to νC=C while νC=N is assigned to the 1573 cm^{-1}. νC–C and νC–N are easily assigned fundamentals, respectively, at 1174 and 1038 cm^{-1}. In this complex the stretching of NO_3^- anion also appears as reasonably well defined mode at 1311 cm^{-1}.

Table 5 summarizes the weight loss and the nature of the peaks measured by, respectively, TG and DTA for the Fe and Co complexes studied in this study. The XRD

Table 5 TG–DTA phenomenological data of the Fe and Co complexes under nitrogen atmosphere

Complex	Stage	TG		DTA	
		T range/°C	Decomposition/%	Peak temp./°C	Nature of peaks
Fe	I	50–140	15.5	122.8	Endo
	II	240–300	72.4	296.5	Exo
Co	I	40–150	20.4	107.8	Exo
	II	230–350	63.3	289.9	Exo
	III	530–600	08.8	574.1	Exo

Table 6 Ignition delay, activation energy for ignition (E^*), and correlation coefficient (r) for Fe and Co complexes (*DNI* Did not ignite)

Complex	D_i/s at temperature/°C						E^*/kJmol^{-1}	r
	290 ± 1	310 ± 1	330 ± 1	350 ± 1	370 ± 1	390 ± 1		
Fe complex	DNI	121	107	90	76	58	28.0	0.984
Co complex	DNI	108	97	82	74	56	24.5	0.977

patterns of the oxides left after thermal decomposition have been shown in Fig. 5. As shown in TG trace of the Fe complex (Fig. 6), two steps decomposition is readily evident. It is noteworthy that DTA also shows an endotherm (122.8 °C) and exotherm (296.5 °C). About 15.5% mass loss is in the temperature range 50–140 °C corresponds to the removal of two nitrate groups and two water molecules whereas, loss of ~72.4% is due to loss of four bipyridine and two nitrate groups (as oxides of nitrogen) leaving iron oxide as residue. As we have mentioned that oxide residue was confirmed by the XRD pattern (Fig. 5). Consideration of these facts gives much mechanistic insight into the decomposition process as-

$$[Fe_2(C_{10}H_8N_2)_4O(OH_2)_2](NO_3)_4 \xrightarrow{-(2H_2O+2NO_2+O_2)} [Fe_2(C_{10}H_8N_2)_4O](NO_3)_2$$

$$[Fe_2(C_{10}H_8N_2)_4O](NO_3)_2 \xrightarrow{-(4C_{10}H_8N_2+2NO_2)} Fe_2O_3 + \text{gaseous products}$$

The connection between structure and bonding in Co complex and its thermolysis characteristics is somewhat complicated by the fact that three step decomposition has taken place. This fact is consistent in the DTA (three exotherms, Table 5) and TG traces. According to TG measurements, Co complex when heated at 10 °C min^{-1} losses 20.4% of its weight between 40 and 150 °C temperature range. The loss of six nitrate groups (as gaseous products) from Co complex corresponds to 21% mass loss. The weight loss (63.3%) in range 230–350 °C is probably due to removal of six bipyridine moieties along with oxygen and water leaving a mixture of CoO and $Co(NO_3)_2$. The chemistry of the third step (550–600 °C) is driven by the combination of $Co(NO_3)_2$ with CoO to generate Co_3O_4. The reaction which summarizes thermal decomposition of Co complex leading to Co_3O_4 (consistant with its XRD data, Fig. 5) is,

$$[Co(C_{10}H_8N_2)_3]_2[Co(OH_2)_6]\cdot 7(OH_2)(NO_3)_8 \xrightarrow{-(6NO_2+3O_2)} [Co(C_{10}H_8N_2)_3]_2[Co(OH_2)_6]\cdot 7(OH_2)(NO_3)_2$$

$$[Co(C_{10}H_8N_2)_3]_2[Co(OH_2)_6]\cdot 7(OH_2)(NO_3)_2 \xrightarrow{-(6C_{10}H_8N_2+\text{gaseous products})} 2CoO + Co(NO_3)_2$$

$$2CoO + Co(NO_3)_2 \longrightarrow Co_3O_4 + \text{gaseous products}$$

Although these complexes are stable at room temperature but, experiences have shown that when subjected to sudden high temperature they ignite. In addition evolution of gases takes place prior to ignition and reddish (Fe_2O_3) and black (Co_3O_4) solid residues are left in the ignition tubes. From the isothermal TG traces (Fig. 7) we can see that after certain fraction of the weight loss the traces remain almost constant, i.e., there is less change in α value with respect to the time. Values of ignition delay and activation energy for ignition are reported in Table 6. Henceforth, the thermal stability of the iron complex is more than the cobalt complex. The plot of $\ln t_{id}$ against $1/T$ is shown in Fig. 8. Ignition becomes inconsistent (no flame appears) before 310 °C (DNI, Table 6). The ignition delay depends exponentially on temperature. The process of ignition [31] can never be treated as steady-state since it is a transient process prior to sustained combustion.

Freeman and Gordon [25] have suggested following heat balance equation in order to evaluate the pre-ignition reactions.

$$dQ_H/dt = d_H/dt - dq/dt \quad (2)$$

where dQ_H/dt is the net rate of heat gain in the system. d_H/dt is the rate of heat produced by pre-ignition reactions, dq/dt is the rate of heat dissipation.The ignition will occur when

$$Q_H = H' \quad (3)$$

where H' = minimum amount of heat required to raise the temperature of the system to the point of ignition. From Eq. 2, it follows

$$Q_H = H - q. \quad (4)$$

where H = total heat produced by pre-ignition reactions. The ignition would occur only if

$$H - q \geq H'$$

The total heat produced by the pre-ignition reactions must be greater than H' by the amount of heat dissipated. Thus

$$H = H' + q \quad (5)$$

The following equation was derived by Freeman and Gordon [25].

$$t_{id} = A\, e^{\Delta H*/RT}. \quad (6)$$

where $\Delta H*$ is the heat of activation and is approximately equal to activation energy (E_a). If the activities of the reactants do not change significantly during pre-ignition reactions, the log of the time of ignition should be a linear function of the reciprocal of the absolute temperature and the relation comes out to be as given in Eq. 1. In this investigation, the values of activation energies for Fe and Co complexes are, respectively, 28.0 and 24.5 kJ/mol^{-1}.

The set of reaction models [32, 33] were used to analyze isothermal TG data (up to 60%, in the range 290–330 °C, Fig. 7) to calculate E_a values for thermal decomposition of Fe and Co complexes. In the model fitting method the kinetics is analyzed by choosing a "best fit" model based on the value of correlation coefficient 'r' close to 1. Among the various values of 'r', calculated for different models the highest value for 'r' for Fe complex corresponds to model 5($r = 0.9989$) which is related to rate controlling process as one dimensional diffusion. For Co complex model 6 ($r = 0.9831$) corresponds to Mampel equation (random nucleation as rate controlling process). The activation energies (from the kinetics analysis of isothermal TG data) for Fe and Co complexes were found to be, respectively, as 63.5 and 38.7 kJ mol^{-1}.

The isoconversional method [34–37] is known to permit estimation of the apparent activation energy; independent of the model, corresponding to extent of conversion of the sample. This method allows the activation energy to be evaluated without making any assumptions about the reaction model. In addition, the method evaluates the effective activation energy as a function of conversion which allows one to explore multistep kinetics. Though model fitting method using a set of reaction model applied to isothermal data but model free approach (isoconversional method) is a better method of obtaining reliable and consistent kinetic information.

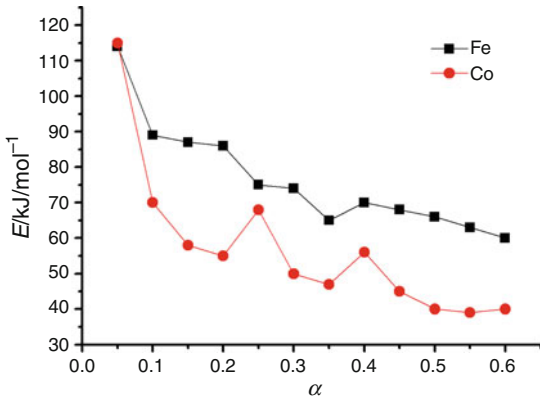

Fig. 9 Plot describing how activation energies ($E*$) value depends on the extent of conversion (α)

According to Fig. 9, each activation energy has a separate value at different α's for both the complexes. Kinetic analysis performed by the isoconversional method on thermogravimetric data has shown (Fig. 9) that thermal decomposition of Fe and Co complexes have initial overall activation energy values 117 and 112 kJ mol^{-1}, respectively. These value decreases with the extent of conversion to about 69 and 45 kJ mol^{-1}, respectively, for Fe and Co complexes at the end of reactions.

Conclusions

The infrared spectroscopic properties of newly prepared complexes of iron and cobalt are in agreement with the result of X-ray crystallography. In both the complexes hydrogen-bonding is limited and obvious. The TG–DTA studies and ignition delay measurements produces highly thermally stable residue which resembles Fe_2O_3 and Co_3O_4 as is consistent with their XRD pattern. For isothermal TG data, use of the isoconversional method is an effective means of unmasking complex kinetics.

Acknowledgements Thanks are due to Head, Department of Chemistry, DDU Gorakhpur University, Gorakhpur for lab facilities. Financial support from UGC and CSIR (Emeritus Scientist) to Dr. Gurdip Singh is highly appreciated. We are grateful to SAIF IIT, Madras for TG–DTA and IR analyses and Chairman, Department of Materials, Indian Institute of Science Bangalore for providing XRD facility.

References

1. Singh G, Pandey DK. Studies on energetic compounds, Part 27: kinetics and mechanism of thermolysis of bis(ethylenediamine) metal nitrates and their role in the burning rate of solid propellants. Propellants Explos Pyro. 2003;28(5):231–9.
2. Singh G, Prem Felix S, Pandey DK. Studies on energetic compounds part:37 kinetics of thermal decomposition of perchlorate complexes of some transition metals with ethylenediamine. Thermochim Acta. 2004;411:61–71.
3. Singh G, Pandey DK. Studies on energetic compounds, part 35: kinetics of thermal decomposition of nitrate complexes of some transition metals with propylenediamine. Combust and Flame. 2003;135:135–41.
4. Singh G, Pandey DK. Studies on energetic compounds, part 40: kinetics of thermal decomposition of bis (propylenediamine) metal perchlorate complexes. J Therm Anal Calorim. 2005;82: 253–60.
5. Singh G, Singh CP, Mannan SM. Thermolysis of some transition metal nitrate complexes with 1,4-diaminobutane ligand. J Hazarad Mater. 2005;122:111–7.
6. Singh G, Singh CP, Mannan SM. Kinetics of thermolysis of some transition metal perchlorate complexes with 1,4-diaminobutane ligand. Thermochim Acta. 2005;437:21–5.
7. Singh G, Baranwal BP, Kapoor IPS, Kumar D, Singh CP, Frohlich R. Preparation, X-ray crystallography and thermal decomposition of some transition metal nitrate complexes with hexamethylenetetramine. J Therm Anal Calorim. 2008;91(3):971–7.
8. Singh G, Baranwal BP, Kapoor IPS, Kumar D, Frohlich R. Preparation X- Ray crystallography and thermal decomposition of some transition metal perchlorate complexes with hexamethylenetetramine. J Phys Chem A. 2007;111:12972–6.
9. Singh G, Singh CP, Mannan SM. Kinetics of thermolysis of some transition metal nitrate complexes with 1,6-diaminohexane ligand. J Hazarad Mater. 2006;A135:10–4.
10. Fedoroff BT, Sheffield OE. In encyclopedia of explosives and related items. Dover: Picatinny Arsenal; 1966. p. F217–F223.
11. Frazer JH, Hicks BL. Thermal theory of ignition of solid propellants. J Phys Chem. 1950;54:872–6.
12. Hicks BL. Theory of ignition considered as a thermal reaction. J Chem Phys. 1954;22:414–20.
13. Kubota N. Survey of rocket propellants and their combustion characteristics. In: Kuo KK, Summerfield M, editors. Fundamental of solid-propellants combustion, progress in Astronautics and Aeronautics, vol 90. Washington DC: AIAA; 1984. Chap 1.
14. Singh G, Kapoor IPS. Thermolysis of AP-additive mixtures III. J Energ Mater. 1993;11:293–310.
15. Singh G, Kapoor IPS, Vasudeva SK. Thermolysis of AP-PS-additive mixtures. Indian J Techn. 1991;29:589–94.
16. Singh G, Singh RR, Rai AP, Kapoor IPS. Thermolysis of AP-PS-additive mixtures I. J Therml Anal Calorim. 1990;36: 2539–46.
17. Singh G, Shrimal AK, Kapoor IPS, Singh CP, Kumar D, Manan SM. Kinetics of thermolysis of some transition metal perchlorate complexes with 1,6-diaminohexane ligand. J Therm Anal Calorim. 2011;103:149–55.
18. Singh G, Kapoor IPS, Kumar D, Singh UP, Goel N. Preparation X-ray crystallography and thermal decomposition of some transition metal perchlorate complexes with perchlorate and 2,2′-bipyridyl ligands. Inorg Chim Acta. 2009;362:4091–8.
19. Sheldrik GM. Phase annealing in *SHELX*-90: direct methods for larger structures. Acta Cryst A. 1990;46:467–73.
20. Sheldrick GM. A short history of *SHELX*. Acta Cryst A. 2008;64:112–22.
21. Klaus B. *DIAMOND*, version 1.2c; Bonn: University of Bonn; 1999.
22. Allen FH. The Cambridge structural database: a quarter of a million crystal structures and rising. Acta Cryst. 2002;B58:380–8.
23. Singh G, Singh RR. Indigenously fabricated apparatus for thermogravimetric analysis. Res Ind. 1978;23:92–3.
24. Semenov N, Chemical kinetics and chain reactions. Oxford: Clarendon Press; 1935. Chap. 18.
25. Freeman ES, Gorden S. The application of the absolute rate theory of the ignition of propagatively reacting systems: thermal ignition of the system, lithium nitrate-magnesium, sodium nitrate-magnesium. J Phys Chem. 1956;60:867–71.
26. Zinn J, Rogers RN. Thermal initiation of explosives. J Phys Chem. 1992;66:2646–53.
27. Singh G, Kapoor IPS. Kinetics of thermolysis of ring-substituted arylammonium nitrates. Combust Flame. 1993;92:283–91.
28. Singh G, Kapoor IPS. Kinetics of thermolysis of ring-substituted arylammonium perchlorates. J Phys Chem. 1992;96:1215–20.
29. Nakamoto K. Infrared and Raman spectra of inorganic and coordination compounds. New York: Wiley; 1978.
30. Carranza J, Sletten J, Lloret F, Julve M. Iron(III), chromium(III) and cobalt(II) complexes with squarate: synthesis, crystal structure and magnetic properties. Inorg Chim Acta. 2011;371:13–9.
31. Zinn J, Roger RN. Thermal ignition of explosives. J Phys Chem. 1962;66:2646–50.
32. Brown ME, Dollimore D, Galway AK. Reactions in the solid state, comprehensive chemical kinetics, vol. 22. Amsterdam: Elsevier. 1960; p. 1–340.
33. Kapoor IPS, Srivastava P, Singh G, Singh UP, Frohlich R. Preparation, crystal structure and thermolysis of phenylenediammonium diperchlorate salts. J Phys Chem A. 2008;112:652–6.
34. Vyazovkin S. A unified approach to kinetic processing of non-isothermal data. Int J Chem Kinet. 1996;28:95–101.
35. Vyazovkin S, Wight CA. Kinetics of thermal decomposition of cubic ammonium perchlorate. Chem Mater. 1999;11:3386–93.
36. Lang AJ, Vyazovkin S. Effect of pressure and sample type on decomposition of ammonium perchlorate. Combust Flame. 2006;145:779–90.
37. Vyazovkin S, Wight CA. Model-fitting approaches to kinetic analysis of isothermal and non-isothermal data. Thermochim Acta. 1999;340:53–68.